HHS Public Access

Author manuscript

Neuroscience. Author manuscript; available in PMC 2021 December 01.

Published in final edited form as:

Neuroscience. 2020 December 01; 450: 3–14. doi:10.1016/j.neuroscience.2020.07.015.

Mutations in ciliary trafficking genes affect Shh-dependent neural tube patterning differentially along the A-P axis.

Emilie Legué[1], **Karel F. Liem Jr.**[1,2,*]

[1]Vertebrate Developmental Biology Program, Department of Pediatrics, Yale School of Medicine, 333 Cedar Street, New Haven, CT 06520

[2]Lead Author

Abstract

Cell specification in the ventral spinal cord is a well-studied model system to understand how tissue pattern develops in response to a morphogen gradient. Ventral cell types including motor neurons (MNs) are induced in the neural tube in response to graded Sonic Hedgehog (Shh) signaling. We performed a forward genetic screen in the mouse that incorporated a GFP-expressing transgene to visualize MNs to identify genes regulating ventral patterning. Here we contrast the neural patterning phenotypes of two mouse lines carrying induced mutations in ciliary trafficking genes. We show that a hypomorphic mutation in the gene *Tubby-like protein 3 (Tulp3)* resulted in a dorsal expansion of MNs consistent with an up-regulation of Shh signaling. Interestingly, patterning defects in *Tulp3* mutants were restricted to posterior regions of the spinal cord as patterning was similar to WT in the anterior spinal cord. In contrast, a mutation in the ciliary trafficking gene *cytoplasmic dynein 2 heavy chain 1 (Dync2h1),* led to a complete loss of MNs in anterior regions of the spinal cord, indicating a strong down-regulation of Shh signaling. However, this severe phenotype was restricted to the cervical region as motor neurons developed posteriorly. Mutations in cilia trafficking genes affect Shh-dependent signaling in the neural tube differentially along the A-P axis in a process that is not understood.

Keywords

Sonic Hedgehog; Tulp3; Dync2h1; spinal cord; dorsal-ventral; mouse

Introduction

Early studies in the Jessell Lab were among the first inquiries into the molecular regionalization of the vertebrate central nervous system, where the major interest at the time was to understand the mechanisms of how neural cells acquire their identity on the dorsal-ventral (D-V) axis of the developing spinal neural tube. These embryological studies were

*Correspondence: Karel.Liem@yale.edu.

conducted in vitro and culminated in an elegant model where neural epithelial cells are induced by signals from the notochord and floor plate that specify ventral character (Jessell, 2000). These signals were mediated by the secreted protein, Sonic Hedgehog (Shh) and ventral neural cell types, including spinal motor neurons and ventral interneurons were induced in response to concentration dependent graded Shh signaling that was opposed by BMP signals which were active dorsally. The floor plate required the highest levels of Shh signaling, while motor neurons (MNs) that developed at a distance from the floor plate required intermediate levels (Roelink et al., 1994). The molecular logic of how ventral cell types are induced in response to Shh has since become a paradigm of how a tissue is patterned in response to a morphogen gradient (Briscoe, 2009). This model was further developed and expanded by Briscoe and colleagues, who demonstrated that Shh functions as a morphogen which acts in a both concentration and temporal manner (Balaskas et al., 2012; Sagner and Briscoe, 2019).

Forward genetic approaches in the mouse that sought to identify genes critical for the patterning of the mammalian body plan uncovered the importance of the primary cilium for the transduction of the Shh signaling pathway (Huangfu et al., 2003) and patterning in the spinal cord. Primary cilia are small microtubule-based organelles that extend from the cell surface of nearly all cells in vertebrates and were previously thought of as vestigial (Pazour et al., 2000). Cilia have since been recognized as critical signaling organelles where components of signaling pathways are enriched. As protein synthesis does not occur within cilia, proteins need to be transported into the cilium. The molecular transport machinery includes the motor proteins, kinesins and dyneins which enable anterograde and retrograde transport on microtubules, respectively. Also critical are the intraflagellar transport (IFT) protein complexes which facilitate the association of ciliary proteins to the motor proteins (Pedersen and Rosenbaum, 2008) (Figure 1A). Mutations in genes encoding proteins that control transport in and out of the cilium have profound effects on the Shh pathway, either up-regulating or down-regulating Shh signaling (Goetz and Anderson, 2010; Sasai and Briscoe, 2012).

The early neural tube is formed by neural progenitor cells organized in a pseudo-stratified columnar epithelium. Progenitor cells span the width of the epithelium and are polarized with the apical aspect of the cells projecting a single primary cilium into the neural tube lumen (Figure 1B–D). Neuroepithelial cells that are exposed to Shh transduce these signals through protein components that are enriched in cilia. These signaling components include the Shh receptor Patched1, the membrane protein Smoothened, the atypical kinesin Kif7, the negative pathway regulator Sufu, as well as the transcription factors that implement the pathway, the Gli proteins (Gli1–3) (Goetz and Anderson, 2010). Hh signaling components show ligand-dependent dynamic trafficking within cilia. The two transcription factors Gli2 and Gli3 are key players in transducing Shh signals as these proteins are localized to the tips of cilia and are processed into activator and repressor forms in a cilia-dependent manner (Goetz and Anderson, 2010; Haycraft et al., 2005). The balance of Gli activator and repressor forms determines the transcription of Shh target genes and thus ventral cell type identity within the neural tube (Briscoe and Therond, 2013). Mutations in genes that disrupt cilia dysregulate the Shh signaling pathway at a step in the pathway downstream of the receptor *Ptch1* and upstream of Gli transcription factors (Goetz and Anderson, 2010).

Here we identified a recessive mutation in the ciliary trafficking gene *Tulp3* (*Tubby-like protein-3*) that disrupted the pattern of early MN induction. The mutation caused an expansion of the MN domain dorsally within the neural tube consistent with an activation of the Shh pathway that was restricted to the caudal region of the spinal neural tube. Little attention has been paid to the interesting phenomenon that the cilia mutations cause alterations in the D-V patterning of the spinal cord differentially along the anterior-posterior (A-P) axis. We compared the D-V patterning phenotype of *Tulp3* mutants with that of a second mutation in a ciliary trafficking gene, the *mei mei* mutation in *cytoplasmic dynein 2 heavy chain 1* (*Dync2h1*). MNs were robustly induced in the neural tube but were absent in rostral regions anterior to the forelimbs in *Dync2h1* mutants. Our studies show that mutations in cilia-related genes can cause defects in Shh signaling in the neural tube that can strongly differ depending on A-P position. This process is not understood in the context of the current models of Shh-dependent patterning but suggests differences in how the ventral neural tube is patterned along the A-P axis.

Results

We took a genetic approach to identify novel regulators of D-V patterning of the spinal cord with a focus on motor neuron (MN) induction and performed an ENU-based mutagenesis screen in the mouse (Liem et al., 2009). To visualize MNs, we utilized a HB9-GFP transgene which labels somatic MNs (Figure 1E) along the anterior-posterior (A-P) axis throughout the motor column from the MNs that form the cranial nerve XII (hypoglossal nerve) anteriorly through the hindlimb region posteriorly. We screened litters for potential homozygous mutations at E10.5 (Liem et al., 2009) and identified a mutant mouse line that displayed diffuse and expanded GFP expression in caudal regions of the spinal cord in embryos that were otherwise morphologically similar to non-affected littermates (Figure 2A,B). We identified a missense mutation leading to the substitution of lysine by isoleucine at position 407 (K407I) in the ciliary trafficking gene *Tulp3* (*Tubby-like protein-3*) (Legue and Liem, 2019). Homozygous mutants went on to develop minor skeletal deformities such as rib duplications as well as kidney cysts at later embryonic stages, consistent with a ciliopathic phenotype (Legue and Liem, 2019).

Tulp3 acts as an adaptor protein that facilitates trafficking of a subset of membrane associated cargo into the primary cilium (Badgandi et al., 2017) (Figure 1A). Tulp3 contains an N-terminal IFT-A (Intraflagellar Transport Protein complex A) binding domain as well as a C-terminal Tubby domain which associates with inositol phosphates (Mukhopadhyay et al., 2010; Santagata et al., 2001).

We next analyzed how the $Tulp3^{K407I}$ mutation affected dorsal-ventral (D-V) patterning in the spinal cord. We examined ventral pattern in cross sections through the developing spinal cord at E10.5 at four A-P levels: (1) cervical (anterior to the forelimb), (2) brachial (forelimb level), (3) thoracic (between the limb buds) and (4) lumbar (hind limb level) using the fluorescence from the HB9-GFP transgene to label MNs and antibodies to FoxA2 to label floor plate cells. We did not detect differences in the D-V patterning of the neural tube between $Tulp3^{K407I/K407I}$ mutant and control embryos at cervical or brachial levels as assessed by the MN and floorplate markers (Figure 3A, B, D, E). However, at thoracic and

lumbar levels, we found a dorsal expansion of the MNs in *Tulp3*$^{K407I/K407I}$ mutants, indicating an up-regulation of Shh signaling. The domain of FoxA2 positive cells was similar in mutant and control embryos, indicating that the increase in Shh signaling was too modest to induce the expansion of the cells requiring the highest levels of Shh signaling (Figure 3G, H, I, K). These data were consistent with a mild Shh gain of function in the *Tulp3*$^{K407I/K407I}$ mutant embryos in caudal regions of the spinal cord.

Previous characterization of the *Tulp3* knockout mouse showed embryonic lethality with strong morphological defects consistent with typical ciliopathic phenotype, including skeleton defects, polydactyly, exencephaly, and a strong up-regulation of Shh signaling in the ventral neural tube (Cameron et al., 2009; Norman et al., 2009; Patterson et al., 2009). Morphologically, *Tulp3*$^{null/null}$ embryos harboring the HB9-GFP transgene displayed an abnormally shaped telencephalon, variable exencephaly, as well as a wavy neural tube at caudal levels (Figure 2C). We examined HB9-GFP fluorescence in *Tulp3*$^{null/null}$ mutants and found expanded diffuse fluorescence in caudal regions of the neural tube (Figure 3D). We examined sections through the neural tube of *Tulp3*$^{null/null}$ mutant embryos and found that the ventral patterning was similar to WT at cervical and brachial levels similar to *Tulp3*$^{K407I/K407I}$ mutant (Figure 3A–F). In contrast, the MNs and floor plate cells were expanded dorsally at the thoracic level indicating a strong up-regulation of Shh signaling in *Tulp3*$^{null/null}$ mutants compared to controls (Figure 3G, I). At the lumbar level, we observed a dorsal expansion of the floor plate and MN domains in the mutants compared to control embryos, greater than at the thoracic level (Figure 3G, I, J, L). These results were consistent with a strong activation of the Shh pathway, similar to previous reports (Cameron et al., 2009; Norman et al., 2009; Patterson et al., 2009). The analysis of the ventral patterning of the neural tube in *Tulp3*^{K407I} and *Tulp3*^{null} homozygous mutants showed that the *Tulp3*^{null} allele had a stronger phenotype than the *Tulp3*^{K407I} allele at the lumbar and thoracic levels, confirming that *Tulp3*^{K407I} was a hypomorphic allele of *Tulp3*. Interestingly, neither the null nor the missense mutations influenced ventral patterning in the anterior spinal regions at this stage. The absence of a phenotype in the anterior regions combined with the dorsal expansion of ventral cell types caudally indicated that loss of *Tulp3* function affected Shh patterning differently at the different A-P regions. Mutations in cilia trafficking genes that affected patterning of the neural tube were often associated with malformations in cilia morphology. We examined *Tulp3*$^{K407I/K407I}$ cilia present on the apical surface of the neuroepithelium by Scanning Electron Microscopy (SEM) of thoracic regions of E10.5 embryos, a region where MNs were expanded. We found that the *Tulp3*^{K407I} mutation did not appear to strongly affect cilia morphology (Figure 4A, B). *Tulp3*^{K407I} cilia appeared slightly shorter and wider (length=672 ±131nm, n=57; width=136±21nm, n=48) compared with WT (length=701 ±177nm, n=94; width 131±26nm; n=47) however these differences were not statistically significant (Figure 4C, D). These observations were consistent with previous studies showing that loss of *Tulp3* function did not strongly affect cilia morphology (Hwang et al., 2019; Legue and Liem, 2019; Patterson et al., 2009).

Mutations in cilia genes in mice cause phenotypes where ventral cell types have been reduced or expanded in the spinal neural tube (Goetz et al., 2009), however little attention has been paid to the interesting phenomenon that alterations in patterning can differ significantly along the A-P axis. To further explore this issue, we analyzed the neural tube

phenotypes in the *mei mei* mouse, another mutant line we identified from the HB9-GFP screen (Liem et al., 2009). *mei mei* harbors a missense mutation in *cytoplasmic dynein 2 heavy chain 1 (Dync2h1^{mmi})*. Dync2h1 is an evolutionarily conserved dynein motor protein that mediates retrograde transport from the cilia tip to the base (Pazour et al., 1999; Signor et al., 1999) (Figure 1A). Previous reports have shown that loss of function mutations in *Dync2h1* resulted in a down-regulation of Shh signaling in the mouse and in tissue culture cells accompanied by abnormal cilia morphology and protein composition (Huangfu and Anderson, 2005; May et al., 2005; Ocbina and Anderson, 2008). *Dync2h1^{mmi}* mutant embryos showed an abnormal telencephalon with variably penetrant exencephaly (Figure 5A, C). We examined the pattern of HB9-GFP expression in *Dync2h1^{mmi}* mutant embryos. Mutants at E9.5 and E10.5 showed abundant MNs except at cervical regions where fluorescence was strikingly reduced anterior to the forelimbs (Figure 5A–D). The absence of MNs anteriorly was also evident by the absence of the hypoglossal nerve (Figure 5D, asterisk). We next analyzed sections through the neural tube at E10.5 at the cervical and thoracic levels. Consistent with the whole-mount observations, we failed to detect GFP-expressing cells at the cervical level of the neural tube in *Dync2h1^{mmi}* mutants compared to controls (Figure 6A, B). We stained sections for the MN marker ISL1/2 which confirmed that few if any motor neurons were present cervical regions of *Dync2h1^{mmi}* mutants (Figure 6C, D). This result was consistent with a strong down-regulation of Shh signaling where neither the cells requiring high or intermediate levels of Shh were specified. However, more caudally the loss of Shh function phenotype was milder as MNs were robustly induced (Figure 5B, D). We found MNs expanded ventrally spanning the midline in a “U” shaped pattern in cross sections at thoracic regions (Figure 6E, F). These studies indicated that in *Dync2h1^{mmi}* mutants the level of Shh signaling was too low to induce MNs anteriorly but was sufficient to induce MNs posteriorly.

While the *Tulp3^{K407I}* mutation did not strongly affect cilia morphology, mutations in *Dync2h1* are associated with severe cilia malformations (May et al., 2005). We tested whether differences in ventral pattern along the A-P axis might derive from a differential effect of the *mei mei* mutation on cilia at the different spinal A-P levels. We first examined WT cilia in the neuroepithelium by SEM and found that cilia morphology was similar in cervical and thoracic regions (Figure 7A, B, E, F). Neural tube cilia in *Dync2h1^{mmi}* mutants were strikingly abnormal appearing engorged and much wider than WT cilia, consistent with ciliary protein accumulation due to defects in retrograde transport (Ocbina et al., 2011) (Figure 7C, D–F). *Dync2h1^{mmi}* mutant cilia appeared similar at both cervical levels where motor neurons failed to develop and thoracic levels where motor neurons were abundant suggesting that differences in Shh activity was not due to a differential effect of the *mei mei* mutation on neuroepithelial cilia at the two A-P levels.

Discussion

Forward genetics is a powerful method to discover new genes and pathways in many biological processes of interest. We incorporated the HB9-GFP transgene developed in the Jessell lab into a genetic screen to aid in the discovery of mutations that affect the pattern of neuron induction in the developing neural tube. The transgene proved useful for the identification of neural patterning mutations in embryos in the absence of morphological

defects, such as the *Tulp3*^{K407I} mutant allele. Moreover, it greatly facilitated the analysis of neural patterning differences at the different A-P levels of the neural tube as it demarcated motor neurons along the entire A-P axis of the spinal cord (Figure 8).

Shh is a morphogen required for the patterning of many tissues including the embryonic ventral spinal cord. Numerous studies have shown that mutations in genes that control ciliary functions can alter Shh signaling in vertebrate animals and cells. Many of the mouse mutants harboring cilia mutations have been analyzed for defects in Shh signaling in the embryonic spinal cord, as it is a region where the role of Shh in developmental signaling is well understood (Huangfu et al., 2003). Loss of function of genes required for cilia biogenesis that ablate the cilium cause a strong loss of function of the Shh pathway and few if any ventral neural cell types are induced in these mutant mice (Goetz and Anderson, 2010; Goetz et al., 2012; Huangfu et al., 2003). However, many proteins are required to build the cilium and mutations in genes that result in an incomplete disruption of cilia structure or function cause partial dysregulation of the Shh pathway. These mutations can result in the expansion or loss of ventral cell types indicating an up- or down-regulation of the pathway. An unexpected feature of the partial dysregulation of the cilium is that Shh-mediated patterning phenotypes in the spinal cord appear to differ considerably at different the A-P levels.

Here we identified a hypomorphic mutation in *Tulp3*, a gene that is required for proper transduction of the Shh signaling pathway and proper patterning of the neural tube. The *Tulp3*^{K407I} mutation caused an expansion of MNs dorsally in the caudal region of the neural tube while anterior regions were unaffected. Interestingly, the phenotype of the null is also restricted to the caudal neural tube (Figure 8). Previous studies showed that loss of function of *Tulp3* resulted in the ectopic expression of the *Gli1-lacZ* reporter, a transcriptional read-out of the Shh signaling pathway, in the caudal neural tube (Cameron et al., 2009). This up-regulation of the Shh pathway included the striking dorsal expansion of FoxA2-expressing floor plate cells, the cell type requiring the highest level of Shh. We show that that up-regulation of Shh signaling contrasted sharply with the absence of phenotype in the more anterior regions in the embryo. Interestingly, protein interaction assays showed that *Tulp3* strongly associated with IFT-A proteins (Mukhopadhyay et al., 2010) and that the expansion of ventral cell types dorsally in the caudal regions of neural tube has also been reported in a number of IFT-A complex mutations: *IFT139*^{aln} (Tran et al., 2008), *IFT122*^{sobp} (Qin et al., 2011), and *IFT144*^{twt} (Ashe et al., 2012; Liem et al., 2012). While these IFT-A mutations resulted in bulged cilia, we found that the *Tulp3*^{K407I} mutation did not cause significant changes in cilia morphology. The mechanisms by which *Tulp3* mutations and *IFT-A* mutations resulted in up-regulation in Shh activity in the caudal neural tube but not in the rostral are likely to be similar.

Differences in Shh-dependent patterning defects along the A-P spinal axis were also observed in other mouse mutations found in the screen. Multiple previous reports have shown that mutations in dynein cause loss of the most ventral structures of the spinal cord such as FoxA2-expressing floor plate cells and Nkx2.2-expressing V3 precursor cells accompanied with MNs expanding ventrally across the midline (Huangfu and Anderson, 2005; May et al., 2005; Ocbina et al., 2011). However, here we show the loss of ventral cell

types is much stronger in the cervical levels compared with other regions of the spinal cord (Figure 8). Similar strong depression of Shh-signaling anterior to the forelimbs was also observed in mouse mutant harboring IFT-A gene mutations that strongly disrupted cilia structure such as *IFT144*^{dmhd} *or IFT144*^{twt}*;IFT122*^{sopb} double mutants (Liem et al., 2012). Interestingly, at lumbar levels, *IFT144*^{dmhd} mutants showed an expansion of MNs both ventrally across the midline as well as dorsally, accompanied by loss of floor plate and Nkx2.2-expressing cells (Liem et al., 2012). Paradoxically, these results showed the simultaneous loss of cells that required the highest levels of Shh signaling, accompanied by the dorsal expansion of MNs indicating an increase in intermediate levels of Shh signaling. This lumbar pattern was also observed in the mouse mutant *henin (Arl13b*^{hnn}*)*, which harbors a mutation in *Arl13b*, a small GTPase required for normal cilia structure (Caspary et al., 2007). Strikingly, the *Arl13b*^{hnn} phenotype was restricted to caudal regions of the spinal cord and the pattern in the anterior spinal cord in *Arl13b*^{hnn} mutants was similar to the WT. It is also important to note that cilia mutations appear to affect ventral patterning along the A-P axis in different ways. For example, the *hop sterile* mutation in *Intraflagellar Transport protein 56* (*IFT56*), a component of the IFT-B protein complex, caused a down-regulation of Shh signaling in the neural tube with a loss of floor plate cells coupled with ventral expansion of MNs. However, this phenotype was restricted to the posterior spinal cord (Xin et al., 2017). This finding contrasts with the phenotypes of *IFT144*^{dmhd} and *Dync2h1*^{mmi} mutants, where the loss of Shh signaling appeared more severe anteriorly.

The mechanism by which mutations in cilia-associated genes cause Shh-mediated patterning defects that affect neuroepithelial cells differentially along the A-P axis of the spinal cord is not understood. One possibility is that the thresholds for the Shh-dependent induction of ventral cell types could differ on the A-P axis of the spinal neural tube. These differences could arise through the influence signaling pathways that specify the anterior-posterior axis of the embryo (Bang et al., 1999; Doniach, 1995; Muhr et al., 1999; Storey et al., 1995) or through differences in developmental timing of the neuroepithelial cells. As the node retracts during embryonic development, new neural tissue is formed such that the anterior neural tube cells have earlier birthdates than posterior cells. Moreover, it has also been shown that the duration and timing of exposure to Shh signaling is an integral component of signaling process that generates the ventral pattern (Dessaud et al., 2007; Sagner and Briscoe, 2019). It is very likely that cilia mutations that dysregulate Shh signaling and act downstream of the ligand-receptor complex would greatly affect the duration and timing of the pathway experienced by neuroepithelial cells. However, a model based on developmental timing alone is complicated by the apparent large patterning differences due to both up and down-regulation of Shh signaling, found in the different A-P positions in the variety of cilia mutants. For example, *Ift56*^{hop}, *IFT144*^{dmhd} and *Dync2h1*^{mmi} mutations all resulted in downregulation of Shh signaling but *Ift56*^{hop} mutants were more affected posteriorly while *IFT144*^{dmhd} and *Dync2h1*^{mmi} mutants were more severely affected anteriorly.

Many Shh signaling proteins localize to primary cilia and differences in ciliary trafficking of these components could potentially account for differential sensitivity to cilia mutations on the A-P axis. However, our studies show that cilia morphology appeared similar in the different A-P regions in WT and in the *Dync2h1*^{mmi} mutants where ventral patterning is differentially affected. Nearly all cells in the vertebrate body have primary cilia and the

genes required for the general process of cilia biogenesis and protein trafficking are in general considered ubiquitously expressed. The detailed analysis of protein trafficking and the dynamic movements of Shh signaling components in cilia is challenging and have been generally performed in tissue culture cells. Differences in cilia structure or ciliary protein composition in different regions of the spinal neuroepithelium have not been previously reported.

Finally, genetic studies in mice testing the requirement of Shh components for neural tube patterning have revealed potential differences in how ventral pattern is established along the A-P axis. MN induction is thought to be Shh dependent and MNs fail to develop in *Shh*$^{-/-}$ embryos (Chiang et al., 1996). However in *Shh;Gli3* double mutant embryos, which lacked both ligand and primary transcriptional repressor, MNs were present but predominantly in the caudal regions of the spinal cord (Litingtung and Chiang, 2000). This result suggested differences in how the pattern is established along the A-P axis, an idea which was also supported by analysis of *Gli2;Gli3* double mutants. All canonical Shh signaling is thought to depend on Gli proteins, the transcriptional transducers of the pathway (Methot and Basler, 2001). *Gli2;Gli3* double mutants lack of both activator and repressor functions and is considered the null state of the Shh pathway, as *Gli1* is not expressed in this genetic context. While *Gli2;Gli3* double mutant embryos were found to lack the floorplate, other ventral cell types including MNs were surprisingly present (Bai et al., 2004; Lei et al., 2004). Interestingly, MNs were found in brachial regions, but were absent at the lumbar regions (Bai et al., 2004; Lei et al., 2004). These data suggested that other pathways were present in the embryo that can induce MNs in the absence of Gli function and canonical Shh signaling, and that the pattern appeared to differ along the A-P axis. While an influence of cilia mutations on non-Shh pathways is formally possible (Satir and Satir, 2019), genetic studies have thus far shown that the effect of cilia mutations on ventral patterning in the different regions of the neural tube is Gli-dependent. Dorsal expansion of ventral cell types in the caudal neural tube of *Tulp3* null embryos depended on *Gli2*, the primary transcriptional activator of the Shh pathway, as *Tulp3*;*Gli2* double mutants did not show expanded MNs and floor plate cells dorsally (Norman et al., 2009). In addition, the failure of MNs to develop in cervical regions in *IFT144*^{dmhd} mutants was dependent on *Gli3*, the primary repressor of the pathway, as *Dmhd;Gli3* double mutants developed motor neurons anterior to the forelimbs (Liem et al., 2012).

In sum, differences in ventral patterning phenotypes along the A-P axis of the spinal neural tube is a common feature of cilia gene mutations, an interesting aspect that has been understudied and may yield insights into how the spinal cord is patterned. We still don’t understand how cilia regulate Gli activators and repressors and a better understanding of this process will greatly help our understanding of how cilia mutations can cause Shh patterning defects in the neural tube that differ along the A-P axis.

Materials and Methods

Mouse strains:

The mouse strains were previously described: *Tulp3*^{K407I} and *Tulp3*^{null} (Legue and Liem, 2019), *HB9-GFP* and *Dync2h1*^{mmi} (Liem et al., 2009). Mice were maintained on the FVB

background. Mice were bred and maintained according to YARC guidelines under an approved IACUC protocol.

Immunofluorescence

Embryos were dissected at the indicated stages (E9.5 or E10.5) and were fixed in 4% PFA on ice for 30 minutes washed in PBS and cryoprotected in 30% sucrose. Prior to embedding, embryos were cut into 4 portions, the cuts were made anteriorly to the fore limb buds, posteriorly to the fore limb buds and anteriorly to the hind limb buds to precisely orient each portion to perform cross sections at the cervical (portion 1), brachial (portion 2), thoracic (portion 3) and lumbar (portion 4) levels. Embryos were embedded in TissueTek (Sakura), frozen and cryo-sectioned at 12μm. Sections were stained using mouse anti-ISL1/2 (1:50) from Developmental Hybridoma Bank (DHB), and rabbit anti-FoxA2 (1:2000) from Abcam primary antibodies and Alexafluor-594 goat anti-rabbit and Alexafluor-594 anti-mouse secondary antibodies (1:500) from Invitrogen. Frozen sections were warmed to room temperature, transferred into PBS and incubated in blocking solution (10% normal goat serum, 0.1% triton PBS) at room temperature for an hour. Sections were incubated in primary antibody in blocking solution O/N at 4°C, rinsed 3 times 5 min in PBS and incubated in secondary antibody in PBS or PBS-DAPI for 2 hours at room temperature, rinsed 3 times 5 min in PBS and mounted in mowiol solution (10% Mowiol 4–88 (Sigma-Aldrich 81381), 25% glycerol, 0.1M Tris). Images were acquired on a Zeiss Axiovert using the Zen software. Whole-mount embryos were imaged on a Zeiss lumar dissecting microscope. The wholemount immunofluorescent embryo was labeled with anti-neurofilament (DHB) and rabbit anti-GFP (Invitrogen) antibodies, dehydrated in methanol and cleared in Benzyl benzoate/Benzyl alcohol and imaged on a Leica TCS SP2 AOBS confocal microscope.

SEM

E10.5 embryos were fixed with 2% PFA and 2.5% glutaraldehyde in 0.1 M sodium cacodylate buffer. Embryos were dissected to expose the luminal surface of the neural tube in 0.1 M cacodylate buffer and dehydrated in ethanol (Huangfu et al., 2003). Scanning electron microscopy was performed and digital images acquired using a FEI ESEM (Figure 4), a Zeiss CrossBeam 550 (Figure 7A,B) or Zeiss Supra25 (Figure 7 C,D) microscope. Cilia measurements were performed using ImageJ. Width was measured at the midpoint of the axoneme length.

Statistical analysis

Comparisons were done using Student t-test (comparison of 2 data sets) or two-way ANOVA followed by Sidak’s test for multiple comparisons (comparison of more than 2 data sets) in Prism8. Statistical significance was attained for p-values <0.05.

Acknowledgments

Tom Jessell was an inspirational advisor. KFL is indebted to Tom for advice and support that spanned 25 years. KFL thanks Kathryn V. Anderson for valuable discussions, support and mentorship. We thank Morven Graham and Nina Lampen for help with S.E.M. KFL is supported by National Institute of Health grant NS097928.

References

Ashe A, Butterfield NC, Town L, Courtney AD, Cooper AN, Ferguson C, Barry R, Olsson F, Liem KF Jr., Parton RG, et al. (2012). Mutations in mouse Ift144 model the craniofacial, limb and rib defects in skeletal ciliopathies. Human molecular genetics 21, 1808–1823. [PubMed: 22228095]

Badgandi HB, Hwang SH, Shimada IS, Loriot E, and Mukhopadhyay S (2017). Tubby family proteins are adapters for ciliary trafficking of integral membrane proteins. The Journal of cell biology.

Bai CB, Stephen D, and Joyner AL (2004). All mouse ventral spinal cord patterning by hedgehog is Gli dependent and involves an activator function of Gli3. Developmental cell 6, 103–115. [PubMed: 14723851]

Balaskas N, Ribeiro A, Panovska J, Dessaud E, Sasai N, Page KM, Briscoe J, and Ribes V (2012). Gene regulatory logic for reading the Sonic Hedgehog signaling gradient in the vertebrate neural tube. Cell 148, 273–284. [PubMed: 22265416]

Bang AG, Papalopulu N, Goulding MD, and Kintner C (1999). Expression of Pax-3 in the lateral neural plate is dependent on a Wnt-mediated signal from posterior nonaxial mesoderm. Developmental biology 212, 366–380. [PubMed: 10433827]

Briscoe J (2009). Making a grade: Sonic Hedgehog signalling and the control of neural cell fate. The EMBO journal 28, 457–465. [PubMed: 19197245]

Briscoe J, and Therond PP (2013). The mechanisms of Hedgehog signalling and its roles in development and disease. Nature reviews Molecular cell biology 14, 416–429. [PubMed: 23719536]

Cameron DA, Pennimpede T, and Petkovich M (2009). Tulp3 is a critical repressor of mouse hedgehog signaling. Developmental dynamics : an official publication of the American Association of Anatomists 238, 1140–1149. [PubMed: 19334287]

Caspary T, Larkins CE, and Anderson KV (2007). The graded response to Sonic Hedgehog depends on cilia architecture. Developmental cell 12, 767–778. [PubMed: 17488627]

Chiang C, Litingtung Y, Lee E, Young KE, Corden JL, Westphal H, and Beachy PA (1996). Cyclopia and defective axial patterning in mice lacking Sonic hedgehog gene function. Nature 383, 407–413. [PubMed: 8837770]

Dessaud E, Yang LL, Hill K, Cox B, Ulloa F, Ribeiro A, Mynett A, Novitch BG, and Briscoe J (2007). Interpretation of the sonic hedgehog morphogen gradient by a temporal adaptation mechanism. Nature 450, 717–720. [PubMed: 18046410]

Doniach T (1995). Basic FGF as an inducer of anteroposterior neural pattern. Cell 83, 1067–1070. [PubMed: 8548794]

Goetz SC, and Anderson KV (2010). The primary cilium: a signalling centre during vertebrate development. Nature reviews Genetics 11, 331–344.

Goetz SC, Liem KF Jr., and Anderson KV (2012). The spinocerebellar ataxia-associated gene Tau tubulin kinase 2 controls the initiation of ciliogenesis. Cell 151, 847–858. [PubMed: 23141541]

Goetz SC, Ocbina PJ, and Anderson KV (2009). The primary cilium as a Hedgehog signal transduction machine. Methods in cell biology 94, 199–222. [PubMed: 20362092]

Haycraft CJ, Banizs B, Aydin-Son Y, Zhang Q, Michaud EJ, and Yoder BK (2005). Gli2 and Gli3 localize to cilia and require the intraflagellar transport protein polaris for processing and function. PLoS genetics 1, e53. [PubMed: 16254602]

Huangfu D, and Anderson KV (2005). Cilia and Hedgehog responsiveness in the mouse. Proceedings of the National Academy of Sciences of the United States of America 102, 11325–11330. [PubMed: 16061793]

Huangfu D, Liu A, Rakeman AS, Murcia NS, Niswander L, and Anderson KV (2003). Hedgehog signalling in the mouse requires intraflagellar transport proteins. Nature 426, 83–87. [PubMed: 14603322]

Hwang SH, Somatilaka BN, Badgandi H, Palicharla VR, Walker R, Shelton JM, Qian F, and Mukhopadhyay S (2019). Tulp3 Regulates Renal Cystogenesis by Trafficking of Cystoproteins to Cilia. Current biology : CB 29, 790–802 e795. [PubMed: 30799239]

Jessell TM (2000). Neuronal specification in the spinal cord: inductive signals and transcriptional codes. Nature reviews Genetics 1, 20–29.

Legue E, and Liem KF Jr. (2019). Tulp3 Is a Ciliary Trafficking Gene that Regulates Polycystic Kidney Disease. Current biology : CB 29, 803–812 e805. [PubMed: 30799240]

Lei Q, Zelman AK, Kuang E, Li S, and Matise MP (2004). Transduction of graded Hedgehog signaling by a combination of Gli2 and Gli3 activator functions in the developing spinal cord. Development 131, 3593–3604. [PubMed: 15215207]

Liem KF Jr., Ashe A, He M, Satir P, Moran J, Beier D, Wicking C, and Anderson KV (2012). The IFT-A complex regulates Shh signaling through cilia structure and membrane protein trafficking. The Journal of cell biology 197, 789–800. [PubMed: 22689656]

Liem KF Jr., He M, Ocbina PJ, and Anderson KV (2009). Mouse Kif7/Costal2 is a cilia-associated protein that regulates Sonic hedgehog signaling. Proceedings of the National Academy of Sciences of the United States of America 106, 13377–13382. [PubMed: 19666503]

Litingtung Y, and Chiang C (2000). Specification of ventral neuron types is mediated by an antagonistic interaction between Shh and Gli3. Nature neuroscience 3, 979–985. [PubMed: 11017169]

May SR, Ashique AM, Karlen M, Wang B, Shen Y, Zarbalis K, Reiter J, Ericson J, and Peterson AS (2005). Loss of the retrograde motor for IFT disrupts localization of Smo to cilia and prevents the expression of both activator and repressor functions of Gli. Developmental biology 287, 378–389. [PubMed: 16229832]

Methot N, and Basler K (2001). An absolute requirement for Cubitus interruptus in Hedgehog signaling. Development 128, 733–742. [PubMed: 11171398]

Muhr J, Graziano E, Wilson S, Jessell TM, and Edlund T (1999). Convergent inductive signals specify midbrain, hindbrain, and spinal cord identity in gastrula stage chick embryos. Neuron 23, 689–702. [PubMed: 10482236]

Mukhopadhyay S, Wen X, Chih B, Nelson CD, Lane WS, Scales SJ, and Jackson PK (2010). TULP3 bridges the IFT-A complex and membrane phosphoinositides to promote trafficking of G protein-coupled receptors into primary cilia. Genes & development 24, 2180–2193. [PubMed: 20889716]

Norman RX, Ko HW, Huang V, Eun CM, Abler LL, Zhang Z, Sun X, and Eggenschwiler JT (2009). Tubby-like protein 3 (TULP3) regulates patterning in the mouse embryo through inhibition of Hedgehog signaling. Human molecular genetics 18, 1740–1754. [PubMed: 19286674]

Ocbina PJ, and Anderson KV (2008). Intraflagellar transport, cilia, and mammalian Hedgehog signaling: analysis in mouse embryonic fibroblasts. Developmental dynamics : an official publication of the American Association of Anatomists 237, 2030–2038. [PubMed: 18488998]

Ocbina PJ, Eggenschwiler JT, Moskowitz I, and Anderson KV (2011). Complex interactions between genes controlling trafficking in primary cilia. Nature genetics 43, 547–553. [PubMed: 21552265]

Patterson VL, Damrau C, Paudyal A, Reeve B, Grimes DT, Stewart ME, Williams DJ, Siggers P, Greenfield A, and Murdoch JN (2009). Mouse hitchhiker mutants have spina bifida, dorso-ventral patterning defects and polydactyly: identification of Tulp3 as a novel negative regulator of the Sonic hedgehog pathway. Human molecular genetics 18, 1719–1739. [PubMed: 19223390]

Pazour GJ, Dickert BL, Vucica Y, Seeley ES, Rosenbaum JL, Witman GB, and Cole DG (2000). Chlamydomonas IFT88 and its mouse homologue, polycystic kidney disease gene tg737, are required for assembly of cilia and flagella. The Journal of cell biology 151, 709–718. [PubMed: 11062270]

Pazour GJ, Dickert BL, and Witman GB (1999). The DHC1b (DHC2) isoform of cytoplasmic dynein is required for flagellar assembly. The Journal of cell biology 144, 473–481. [PubMed: 9971742]

Pedersen LB, and Rosenbaum JL (2008). Intraflagellar transport (IFT) role in ciliary assembly, resorption and signalling. Current topics in developmental biology 85, 23–61. [PubMed: 19147001]

Qin J, Lin Y, Norman RX, Ko HW, and Eggenschwiler JT (2011). Intraflagellar transport protein 122 antagonizes Sonic Hedgehog signaling and controls ciliary localization of pathway components. Proceedings of the National Academy of Sciences of the United States of America 108, 1456–1461. [PubMed: 21209331]

Roelink H, Augsburger A, Heemskerk J, Korzh V, Norlin S, Ruiz i Altaba A, Tanabe Y, Placzek M, Edlund T, Jessell TM, et al. (1994). Floor plate and motor neuron induction by vhh-1, a vertebrate homolog of hedgehog expressed by the notochord. Cell 76, 761–775. [PubMed: 8124714]

Sagner A, and Briscoe J (2019). Establishing neuronal diversity in the spinal cord: a time and a place. Development 146.

Santagata S, Boggon TJ, Baird CL, Gomez CA, Zhao J, Shan WS, Myszka DG, and Shapiro L (2001). G-protein signaling through tubby proteins. Science 292, 2041–2050. [PubMed: 11375483]

Sasai N, and Briscoe J (2012). Primary cilia and graded Sonic Hedgehog signaling. Wiley interdisciplinary reviews Developmental biology 1, 753–772. [PubMed: 23799571]

Satir P, and Satir BH (2019). The conserved ancestral signaling pathway from cilium to nucleus. Journal of cell science 132.

Signor D, Wedaman KP, Orozco JT, Dwyer ND, Bargmann CI, Rose LS, and Scholey JM (1999). Role of a class DHC1b dynein in retrograde transport of IFT motors and IFT raft particles along cilia, but not dendrites, in chemosensory neurons of living Caenorhabditis elegans. The Journal of cell biology 147, 519–530. [PubMed: 10545497]

Storey KG, Selleck MAJ, and Stern CD (1995). Neural Induction and Regionalization by Different Subpopulations of Cells in Hensens Node. Development 121, 417–428. [PubMed: 7768183]

Tran PV, Haycraft CJ, Besschetnova TY, Turbe-Doan A, Stottmann RW, Herron BJ, Chesebro AL, Qiu H, Scherz PJ, Shah JV, et al. (2008). THM1 negatively modulates mouse sonic hedgehog signal transduction and affects retrograde intraflagellar transport in cilia. Nature genetics 40, 403–410. [PubMed: 18327258]

Xin D, Christopher KJ, Zeng L, Kong Y, and Weatherbee SD (2017). IFT56 regulates vertebrate developmental patterning by maintaining IFTB complex integrity and ciliary microtubule architecture. Development 144, 1544–1553. [PubMed: 28264835]

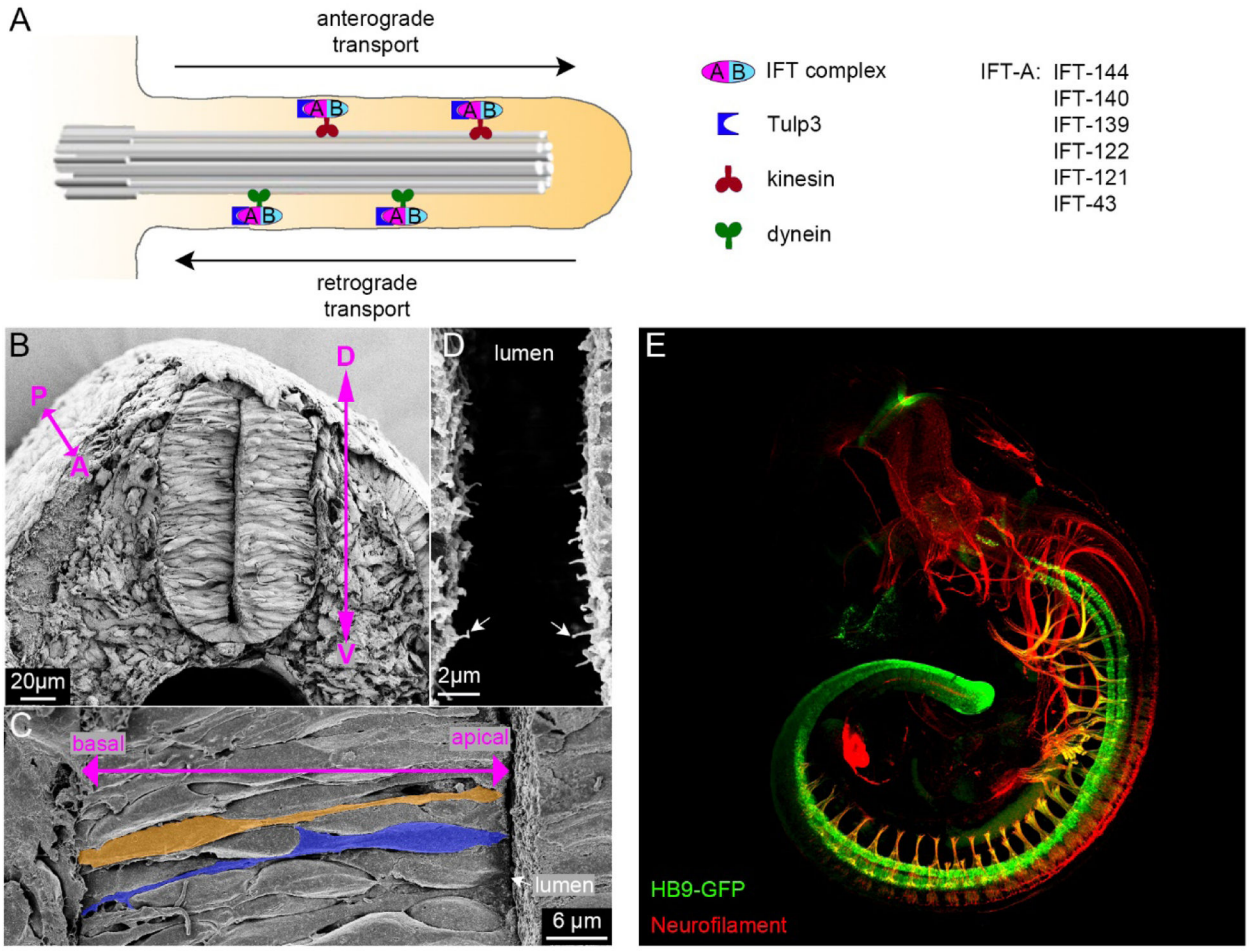

Figure 1: Ciliated neuroepithelial cells of the mouse neural tube

A: Schematic of a primary cilium and the intraflagellar transport (IFT) machinery. The IFT particle consists of two complexes, IFT-A and IFT-B. IFT associates with kinesin motor proteins for anterograde transport of cargo proteins into the cilium and associates with dynein motor proteins during retrograde transport out of the cilium. Tulp3 associates with IFT-A proteins to bring a subset of membrane-associated proteins into the cilium. Members of the IFT-A complex are listed. **B**: Scanning electron microscopy SEM image of cross section of a mouse neural tube at embryonic day 9.5 (E9.5). D=dorsal, V=ventral, A=anterior, P=posterior **C**: The neuroepithelium of the neural tube is pseudostratified with polarized neural progenitor cells extending processes to both the basal and apical aspects of the neural tube. The nuclei of cycling progenitors oscillate between apical and basal aspect of the cell (interkinetic nuclear migration) and newly differentiated cells exit the cell cycle and move to the lateral aspect of the tube. **D**: Each neuroepithelial cell projects a single primary cilium from its apical surface into the lumen of the neural tube, shown here at E10.5. Two examples of cilia are marked by arrows. **E**: Immunofluorescent image of a cleared E10.5 embryo expressing HB9-GFP transgene stained for GFP (green) and neurofilament (red).

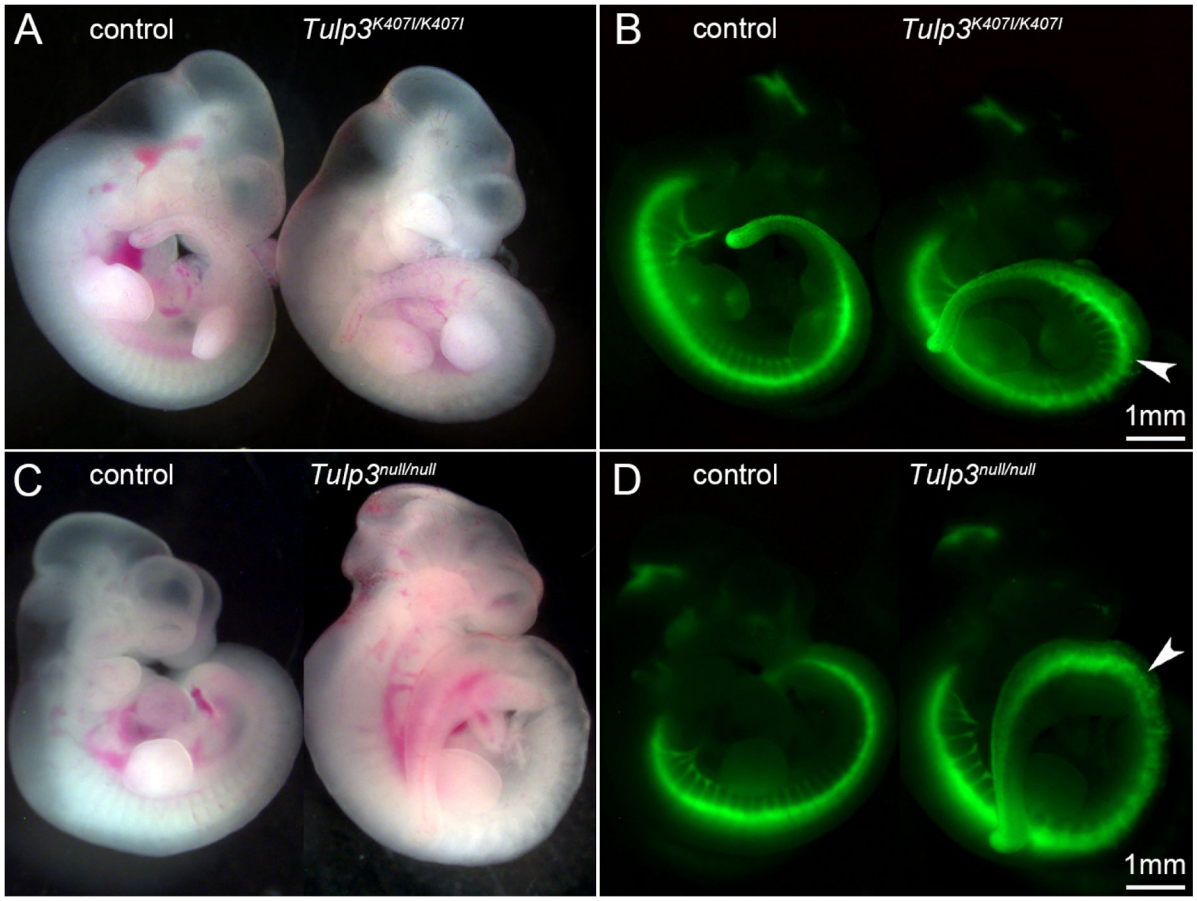

Figure 2: *Tulp3* mutants show dorsal expansion of motor neurons in the posterior neural tube

A: Bright-field images of E10.5 control and *Tulp3*$^{K407I/K407I}$ embryos carrying the HB9-GFP transgene showing no obvious morphological defects in the mutant compared to control. **B**: fluorescence image of the embryos shown in A showed a diffuse pattern of GFP expression in the *Tulp3*$^{K407I/K407I}$ embryo in the neural tube in posterior regions (arrowhead) compared to controls while the anterior GFP pattern appeared similar to controls. **C**: Bright-field image of E10.5 control and *Tulp3*$^{null/null}$ embryos showing morphological defects in the mutant. **D**: fluorescence image of embryos shown in C showed motor neuron expansion dorsally in posterior neural tube (arrowhead) in the *Tulp3*$^{null/null}$ embryo while the anterior neural tube was similar to controls.

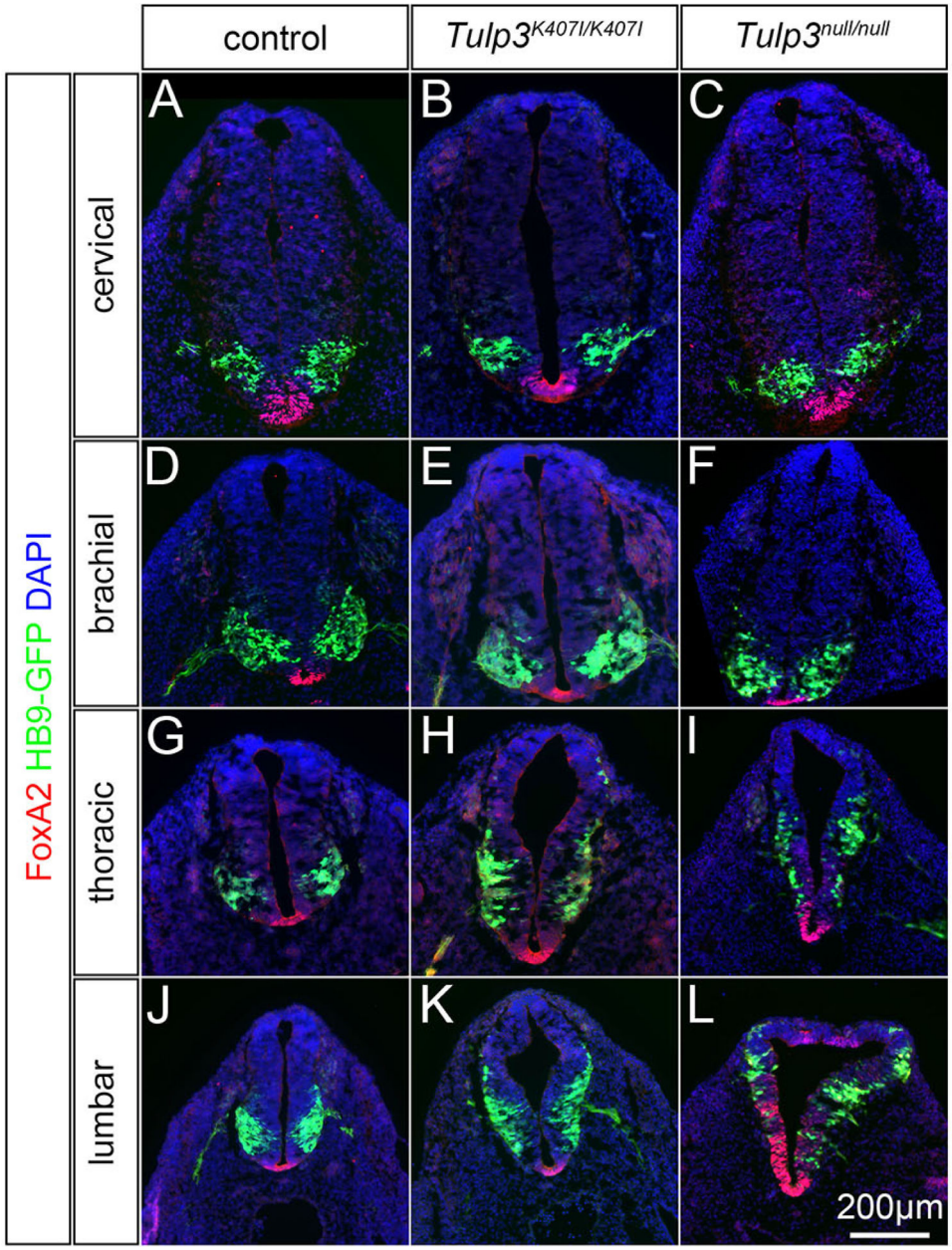

Figure 3: *Tulp3* mutant neural tubes are ventralized in posterior regions

A-L: Cross-sections through neural tubes of E10.5 embryos expressing HB9-GFP (green) and strained for FoxA2 (red) to mark the floor plate domain taken at the cervical (A-C), brachial (D-F), thoracic (G-I) and lumbar (J-L) levels. Control (A D, G, J), *Tulp3*$^{K407I/K407I}$ (B, E, H, K) and *Tulp3*$^{null/null}$ (C, F, I, L) embryos are shown. Nuclei were stained by DAPI (blue). The mutant embryos appeared similar to control at the cervical and brachial levels (A-F). The *Tulp3*$^{K407I/K407I}$ embryo displayed a dorsal expansion of the motor neuron domain but the floor plate domain was similar to control at both thoracic and lumbar levels compared to control (G, H, J, K). The *Tulp3*$^{null/null}$ embryo showed an expansion of both the motor neuron and the floor plate domains dorsally at the thoracic and lumbar levels compared to control (G, I, J, L).

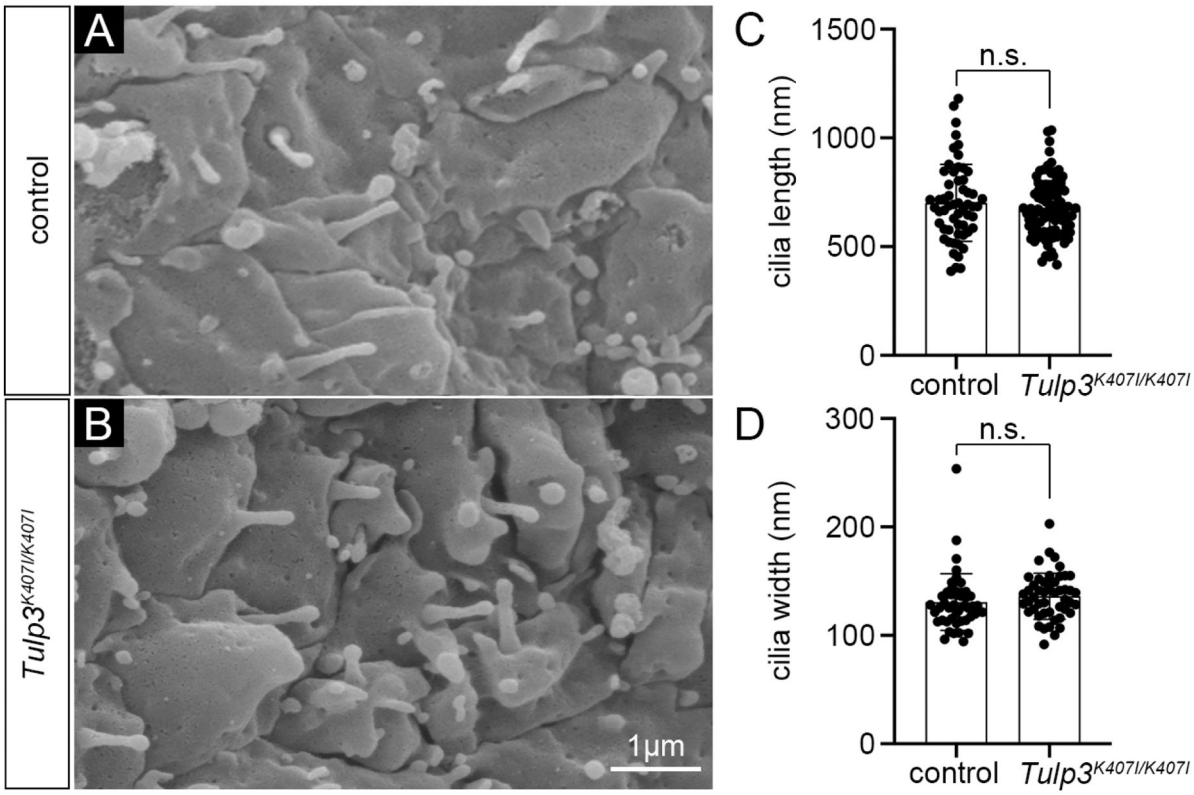

Figure 4: The *Tulp3* ^{K407I} mutation does not strongly affect neural tube cilia morphology

A, B: Scanning electron microscopy images of E10.5 neural tube cilia on the apical surface of control (A) and *Tulp3*$^{K407I/K407I}$ (B) embryos at thoracic levels, viewed en face. **C, D**: Measurements of apical cilia. The measured length (C) and width (D) of individual cilia did not show significant differences between control (WT) and *Tulp3*$^{K407I/K407I}$. Mean +/− s.d. are shown. Statistical differences were calculated using Student's t-test, statistical significance was set at $p<0.05$.

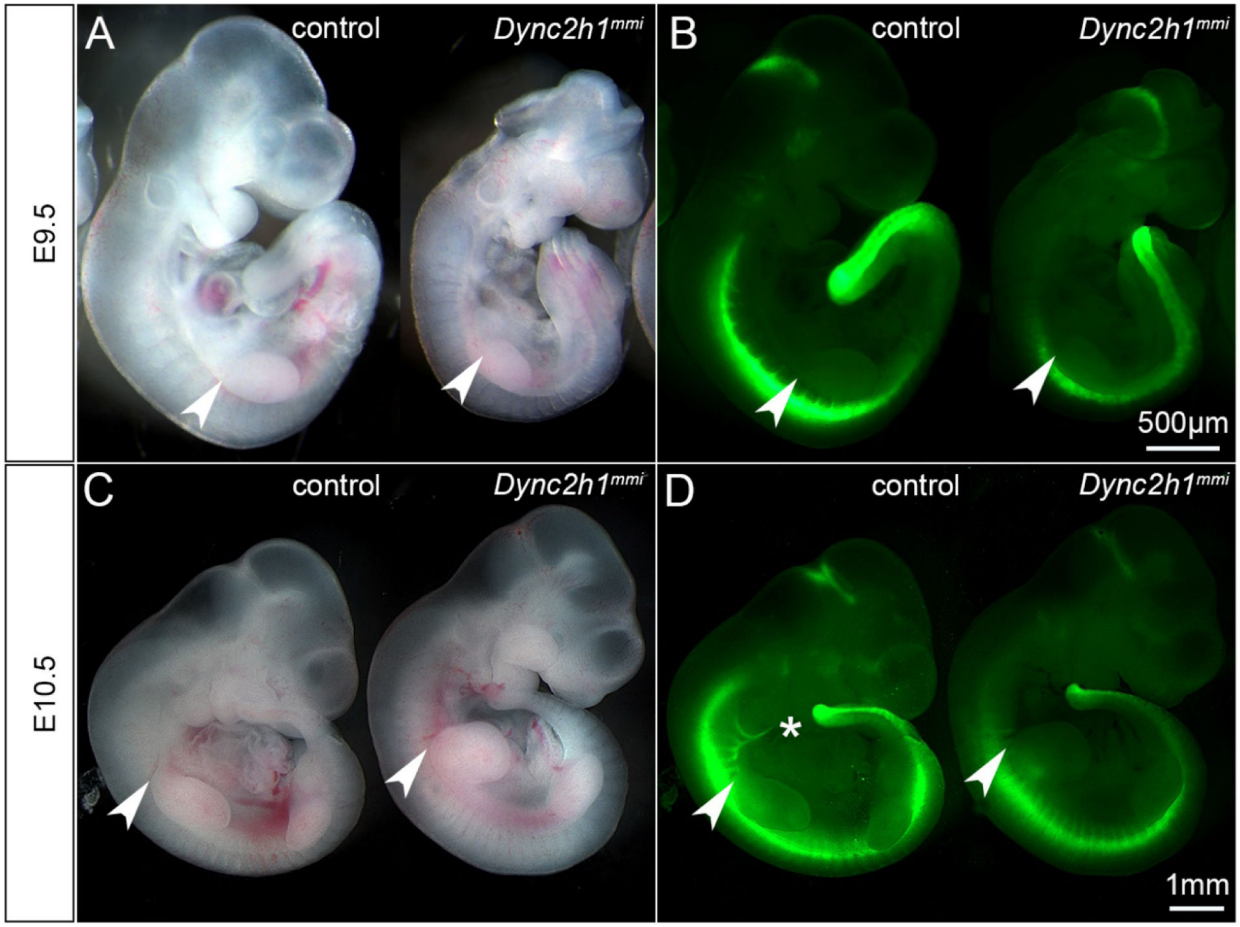

Figure 5: *Dync2h1*^{mmi} mutant embryos lack motor neurons anteriorly

A: Bright field image of E9.5 control and *Dync2h1*^{mmi} embryos harboring the HB9-GFP transgene. **B**: Fluorescent image of the same embryos as in A. **C**: Bright field image of E10.5 control and *Dync2h1*^{mmi} embryos harboring the HB9-GFP transgene. **D**: Fluorescent image of the same embryos as in C. Note the absence of GFP-expressing motor neurons anterior to the forelimbs in *Dync2h1*^{mmi} mutants (arrowhead). Note the loss of the hypoglossal nerve in *Dync2h1*^{mmi} embryos at E10.5 (asterisk).

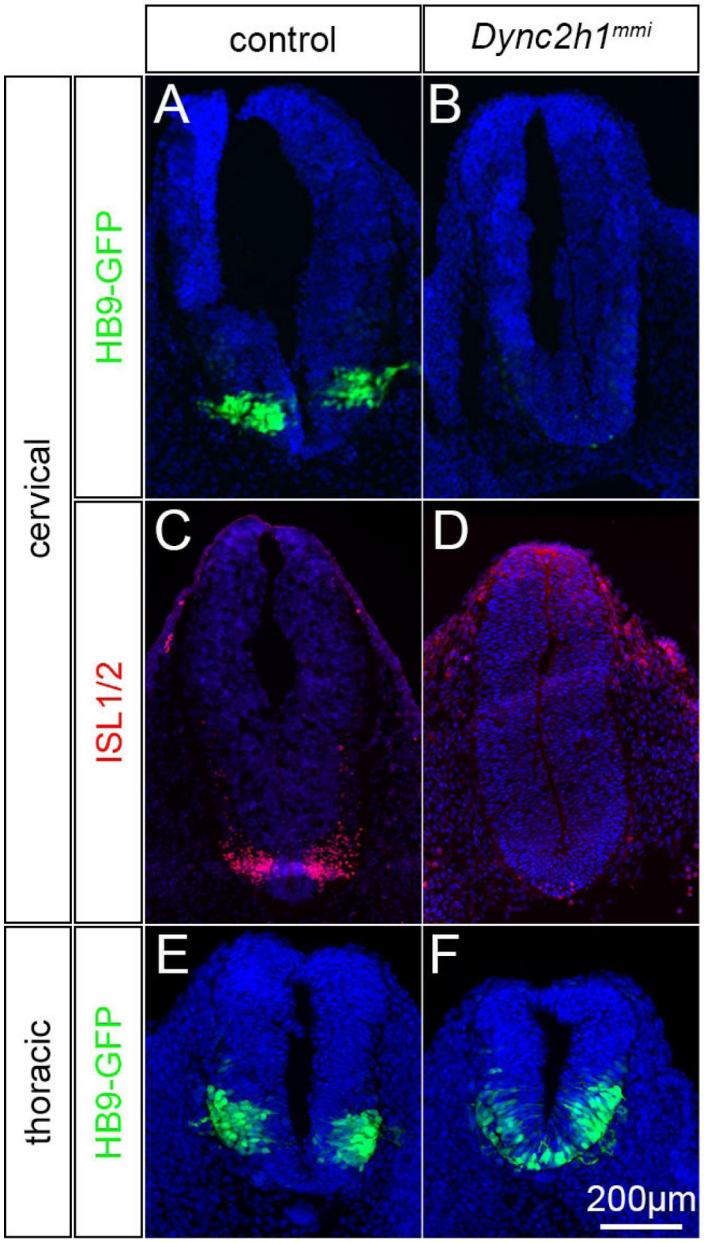

Figure 6: Motor neurons fail to be induced anteriorly but develop and are expanded ventrally in *Dync2h1*^{mmi} embryos

A-D: Cross-sections of neural tube of control and *Dync2h1*^{mmi} E10.5 embryos taken at cervical levels. HB9-GFP fluorescence showed that motor neurons were absent at the cervical level in the *Dync2h1*^{mmi} embryos (A, B). Absence of motor neurons was confirmed by ISL1/2 staining which labels motor neurons (C, D). **E, F**: Cross-sections of neural tube of control and *Dync2h1*^{mmi} E10.5 embryos taken at thoracic levels. HB9-GFP fluorescence show motor neurons that spanned the ventral aspect of the neural tube in the *Dync2h1*^{mmi} embryos.

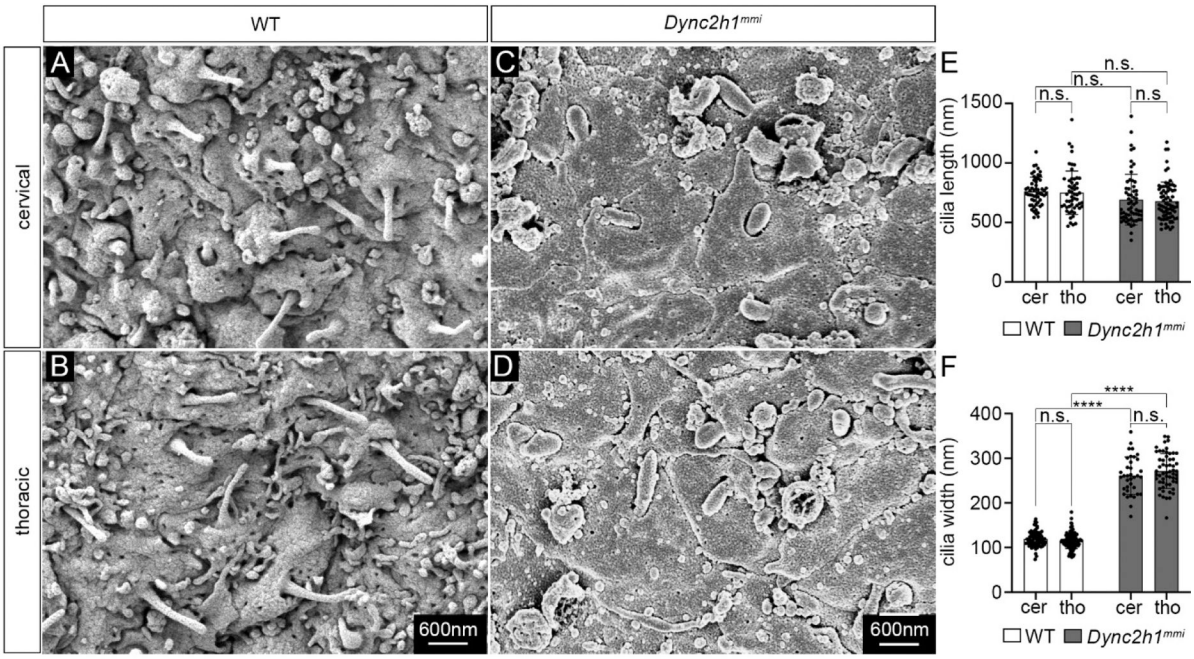

Figure 7: Neural tube cilia in *Dync2h1*^{mmi} embryos are similar at the cervical and thoracic levels.

A-D: Scanning electron microscopy image of neural tube cilia of WT and *Dync2h1*^{mmi} E10.5 embryo at the cervical (A, B) and thoracic (C, D) levels showing abnormally shaped thickened cilia in the *Dync2h1*^{mmi} mutant at both levels. **E, F**: Quantification of the length (E) and width (F) of the cilia in WT and *Dync2h1*^{mmi} mutant neural tubes at the cervical and thoracic levels. **E:** WT cervical length 761±120nm (n=56); thoracic length 751±182nm (n=54) compared with *Dync2h1*^{mmi} cervical length 692±212nm (n=61) and thoracic length 679 ±160nm (n=73). **F:** WT cervical width 115±17nm (n=74) and thoracic width 119±17nm (n=116) compared with *Dync2h1*^{mmi} cervical width 261±42nm (n=36) and thoracic width 272±39nm (n=57). While *Dync2h1*^{mmi} cilia were wider than WT cilia at both cervical and thoracic levels, we did not detect statistical differences in either WT or *Dync2h1*^{mmi} cilia at the cervical versus thoracic levels. Statistical differences were calculated using two-way ANOVA followed by Sidak's test for multiple comparisons, statistical significance was set at $p<0.05$. cer: cervical; tho: thoracic.

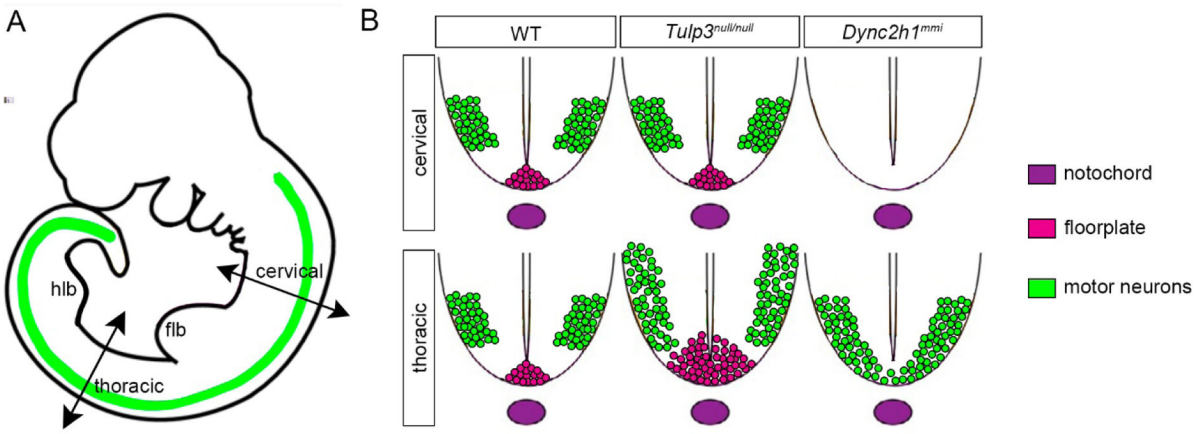

Figure 8: Mutations in cilia trafficking genes differentially affect dorsal-ventral patterning of the spinal neural tube along the anterior-posterior axis

A: Schematic of a E10.5 embryo showing the positions of the cervical and thoracic cross sections. The HB9-GFP expression is shown in green. **B**: organization of motor neurons and floor plate cells in cross sections of WT, *Tulp3*$^{null/null}$ and *Dync2h1*^{mmi} E10.5 embryos at cervical and thoracic levels. In the *Tulp3*$^{null/null}$ embryo, motor neurons and floor plate cells were expanded dorsally in the posterior but not in the anterior part of the neural tube, consistent with an up-regulation of Shh signaling posteriorly. Similar phenotypes are seen in the *IFT144*^{twt}, *IFT139*^{aln}, and *IFT122*^{sopb} mutant mice (Liem et al., 2012; Qin et al., 2011; Tran et al., 2008). In the *Dync2h1*^{mmi} embryo, motor neurons or floor plate cells were absent anteriorly (at cervical levels) indicating a strong loss of Shh signaling while motor neurons were spanning the ventral aspect of the neural tube more posteriorly, indicating that intermediate levels of Shh signaling were present posteriorly. A similar phenotype was seen in *IFT144*^{dmhd} (Liem et al., 2012). Flb=forelimb bud; hlb=hindlimb bud.